New Possibilities for Tuning Ultrathin Cobalt Film Magnetic Properties by a Noble Metal Overlayer

M. Kisielewski, A. Maziewski,* and M. Tekielak
Institute of Experimental Physics, University of Bialystok, Lipowa 41, 15-424 Bialystok, Poland

A. Wawro and L. T. Baczewski
Institute of Physics, Polish Academy of Sciences, Aleja Lotników 32/46, 02-668 Warsaw, Poland
(Received 19 April 2002; published 6 August 2002)

Complementary multiscale magneto-optical studies based on the polar Kerr effect are carried out on an ultrathin cobalt wedge covered with a silver wedge and subsequently with the Au thick layer. A few monolayers of Ag are found to have a substantial effect on magnetic anisotropy, the coercivity field, and Kerr rotation. The silver overlayer thickness-driven magnetic reorientation from easy axis to easy plane generates a new type of 90° magnetic wall for cobalt thicknesses between 1.3 and 1.8 nm. The tuning of the wall width in a wide range is possible. Tailoring of the overlayer structure can be used for ultrathin film magnetic patterning.

DOI: 10.1103/PhysRevLett.89.087203 PACS numbers: 75.30.Gw, 75.60.Ch, 75.60.Ej, 75.60.Jk

Ferromagnetic ultrathin films have been the object of intensive studies because of their unique physical properties and possible applications for magnetic storage media and giant magnetoresistance sensors. Magnetic reorientation phase transition (RPT) in ultrathin films has been one of the challenging topics of recent studies. Thickness-dependent properties and modification of surface or interface film structure give tremendous opportunities for material engineering [1] unattainable in bulk material. Thickness-driven RPT was initially investigated in iron and cobalt films [2,3]. In-plane magnetic anisotropy tailoring by submonolayer cover Cu layer has been reported for Co/Cu systems [4,5]. The influence of various cover layers of Au, Cu, Pd, Pt, Ag, and W on perpendicular magnetic anisotropy [6–9], as well as the strong increase of RPT thickness induced by carbon contamination [10], has been investigated in cobalt ultrathin films. Also the relation between substrate roughness and RPT has been analyzed [11]. However, the results mentioned above have been acquired in measurements carried out *in situ*, which have a limited technical potential for complex and complementary magnetic investigation. Samples available only in an ultrahigh vacuum, although very important in basic research, are not promising in practical applications.

Ex situ study of samples with nonmagnetic overlayer-induced changes of their magnetic properties was the aim of the present Letter. The overlayer spatial structure should, through anisotropy changes, induce a 90° wall between the perpendicular and in-plane domain and thus enable film patterning. An important problem recently investigated is the lateral patterning of ultrathin magnetic films performed, e.g., by ion implantation [12], by substrate surface single-crystal polycrystal modulation [13], or by introduction of a correlated defect [14]. An overlayer structure—a silver wedge layer covered by gold—was chosen as the object of study, because of the different contributions of Au and Ag coverage of cobalt film to magnetic anisotropy [1]. A spatially resolved investigation of wedge-shaped structures is a very ingenious way to probe the thickness-dependent properties. Co and Ag double-wedged samples with mutually perpendicular slope directions were produced in this work. Magneto-optical magnetometry is a very powerful local probing technique, therefore polar—Kerr—effect based magnetometers were used for complementary magnetic ordering analysis performed in both millimeter and micrometer scales.

The samples were prepared in a molecular beam epitaxy system operating in the low range of 10^{-10} Torr vacuum equipped with effusion cells and electron guns. Growth process was monitored *in situ* by reflection high-energy electron diffraction (RHEED) and Auger-electron spectroscopy. A 10 mm × 10 mm polished sapphire Al_2O_3 (11–20) single-crystal wafer was used as a substrate. The (110) Mo buffer layer of 20 nm in thickness was grown at 1000 °C. Next the 20 nm thick Au layer was deposited at room temperature onto the Mo buffer. A Mo(110) buffer imposes the (111) Au growth, which has been monitored by RHEED. Then the following structure was grown (see the inset in Fig. 1): (i) the Co wedge changes thickness (d) from 0 to 2 nm along the "x" axis ; (ii) thickness h of the Ag wedge increases along the "y" axis from 0 at $y =$ 3 mm to 6 nm at $y = 7$ mm and above this coordinate is kept constant, and (iii) 8 nm thick gold covers the whole sample. The "gold region" Au/Ag(0 nm)Co(d)/Au/Mo/Al_2O_3 ($y < 3$ mm) and the "silver region" Au/Ag(6 nm)/Co(d)/Au/Mo/Al_2O_3 ($y > 7$ mm) are distinguished in the sample. In respect to magnetic properties, both Au buffer and Au cover layers can be treated as bulk ones.

Measurements were performed at room temperature by polar Kerr effect using both (i) a magneto-optical magnetometer for study in the millimeter range of the gold and silver regions taken as reference areas and (ii) an optical microscope for micromagnetometry. A classical glass-rod-based technique was applied for light polarization modulation and Kerr rotation angle compensation in the magnetometer. A reflected light beam ($\lambda = 650$ nm) was

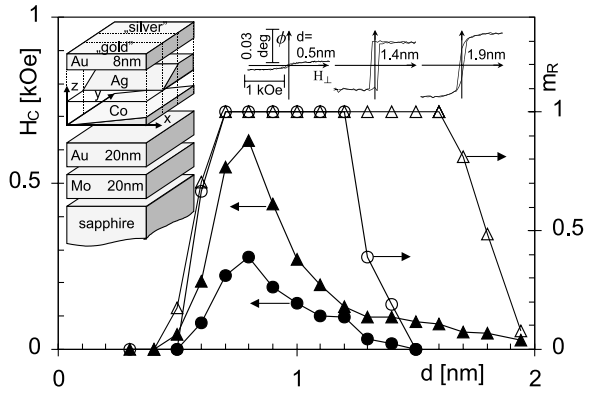

FIG. 1. Coercivity field H_C (full symbols) and remnant normalized magnetization m_R (open symbols) determined as a function of d in the gold (triangles) and silver (circles) regions. The inset shows typical hysteresis loops measured at different d for the gold area. A schematic view of the double wedge sample is also shown.

passed through a 1 mm wide slit in order to limit a sample area. The acquisition of Kerr rotation angle φ and control of both components of applied magnetic field $H_\perp$ perpendicular and $H_\parallel$ parallel to the Co film plane were done by a computer. The domain structure study was performed by an optical polarization microscope with halogen lamp illumination and a cooled CCD camera with a resolution of 1300×1030 pixels.

The Kerr rotation angle $\varphi(H_\perp, H_\parallel = \text{const})$ was measured locally in both the gold and silver regions for different d. The coercivity field $H_C(d)$ determined from hysteresis loops $\varphi(H_\perp, H_\parallel = 0)$ is shown in Fig. 1. This figure also depicts the thickness dependence of a normalized perpendicular component of remanence magnetization m_R [$m_R = \varphi(H = 0)/\varphi_{\max}$]. Maximal Kerr rotation $\varphi_{\max}$ linearly increases with d, similarly to observations performed in Au/Co/Au sandwiches deposited on glass [6,15]. The $\varphi_{\max}$ approaches zero with decreasing d to about a single Co monolayer in both the gold and silver regions. The slope of $\varphi_{\max}(d)$ in the gold region is higher by a factor of 1.7 in comparison to the silver one.

Magnetic anisotropy $K_{1\text{eff}}$ and K_2 constants were determined by fitting theoretical curves to experimental data $\varphi(H_\perp, H_\parallel = \text{const})$, assuming that the magnetic film total energy $E_{\text{tot}}(\theta)$ is expressed by the following standard formula: $E_{\text{tot}}(\theta) = -H_\perp M_S \cos(\theta) - H_\parallel M_S \sin(\theta) + K_{1\text{eff}} \sin^2(\theta) + K_2 \sin^4(\theta)$, where the θ angle is measured from the sample normal direction. The standard, phenomenological relations based on Néel predictions $K_{1\text{eff}}(d) = -2\pi M_S^2 + K_{1v} + 2K_{1sm}/d$ is used containing the demagnetization term and two anisotropy constants (volume K_{1v} and mean surface K_{1sm} originating from the interfaces with buffer and overlayer). The dependence of $K_{1\text{eff}}(d)$ for both regions is plotted in Fig. 2. Mean surface anisotropy constant K_{1s} and volume anisotropy constant K_{1v} were fitted to $K_{1\text{eff}}(d)$ taking the saturation magnetization of the Co film $M_S = 1420$ G s. Within experimental error, the volume anisotropy constants have the same values in both regions. However, the surface contribution substantially differs. The values of the K_2 constant are positive for both regions. Based on the relation between the anisotropy constants, three states of magnetic ordering are distinguishable with the increase of d. For $d < d_1$, where d_1 is defined as $K_{1\text{eff}}(d_1) = 0$, magnetization is perpendicular to the sample plane (easy axis state). In the range of Co thicknesses between d_1 and d_2, $[K_{1\text{eff}}(d_2) = -2K_2]$, the magnetization vector rotates from the normal direction towards the film plane (easy cone). Finally, for $d > d_2$, magnetization is aligned in the film plane (easy plane). All three magnetic ordering states distinguished above are schematically shown in Fig. 2.

Spatial distribution of the remnant state is studied by our micromagnetometer on the basis of $I(i, j)$ image matrix registered by the CCD camera, where i, j are related to the (x, y) coordinates of an analyzed point on the sample surface, upon application of field $H_\perp$. The normalized differential image defined as $P(i, j) = [I_+(i, j) - I_-(i, j)]/[I_+(i, j) + I_-(i, j)]$ is shown in Fig. 3, where I_+ and I_- denote images recorded after sample saturation in $H_\perp > 0$ and $H_\perp < 0$, respectively. The gray level of the pixel is proportional to the local values of both the normalized remnant magnetizations m_R and $\varphi_{\max}$. Three areas are clearly distinguishable in the map of the remnant state—two black regions surrounding a bright one. Figures 3(b) and 3(c) show a linear dependence of the $P(i, j)$ signal on d in the gold and silver areas where $m_R = 1$. The d_{RL} (''low'') and the d_{RH} (''high'') thicknesses, which define the borders of the bright ($m_R = 1$) area, are marked in the

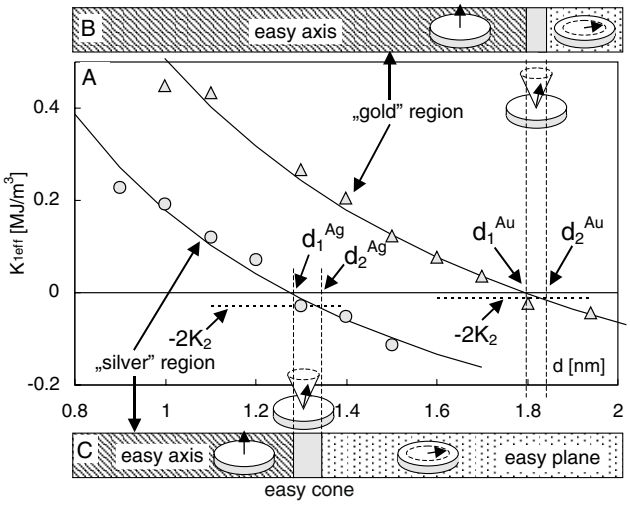

FIG. 2. $K_{1\text{eff}}$ anisotropy constants determined for different d at the silver (circles) and gold (triangles) areas. Solid $K_{1\text{eff}}(d)$ curves were fitted with $K_{1s} = (0.57 \pm 0.03)$ mJ/m^2, $K_{1v} = (0.63 \pm 0.04)$ MJ/m^3 for the gold region and $K_{1s} = (0.42 \pm 0.04)$ mJ/m^2, $K_{1v} = (0.62 \pm 0.06)$ MJ/m^3 for the silver region. Magnetic state diagrams (B and C) were constructed for both regions using horizontal dashed lines representing averaged $-2K_2$ values.

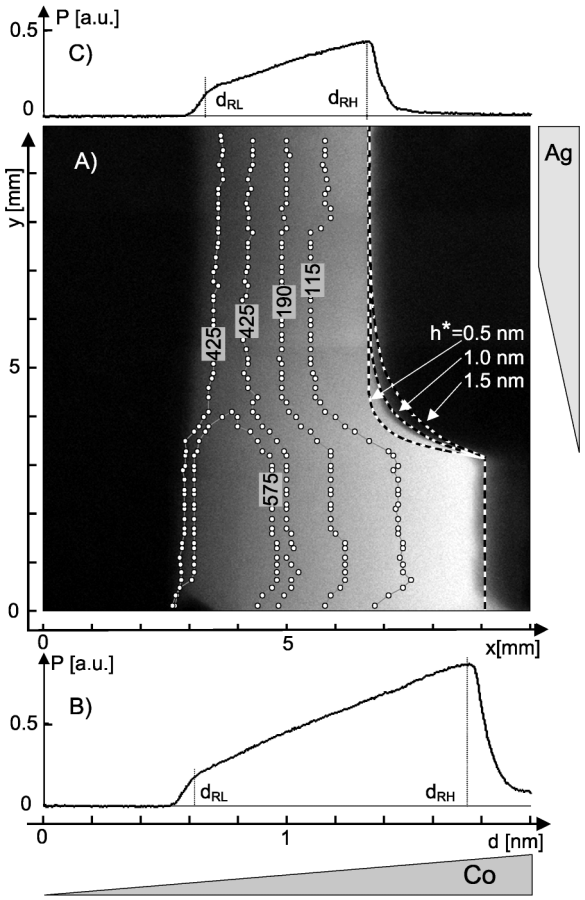

FIG. 3. Remanent state analysis. (A) The cobalt wedge image $P(i, j)$ determined for a fully saturated sample in both directions. The dashed lines $K_{1\text{eff}}(x, y) = 0$ curves were calculated for anisotropy constants taken from Fig. 2 and $h^* = 0.5$, 1, 1.5 nm. Circles show the coercivity wall positions registered for different $H_\perp$ field amplitudes (measured in Oe). (B) and (C) Image intensity profiles $P[d(x)]$ calculated along the wedge in the gold and silver regions, respectively.

profiles in Fig. 3. A steeper decrease of $P(i, j)$, below $d_{RL}(y)$, is associated with the lowering of both $\varphi_{\max}$ and m_R values (see Fig. 1). $P(i, j)$ finally vanishes approaching the low thickness black area, where the sample is in its ideal soft ferromagnetic state followed by a superparamagnetic one for the smallest d. The d_{RL} only weakly depends on y, which is evidence that low Co thickness magnetic properties are mainly determined by layer morphology and that the influence of the Ag/Au interface is negligible. Rapid $P(i, j)$ decrease also occurs for high Co thickness above the $d_{RH}(y)$, i.e., approaching the region of RPT. The overlayer structure substantially affects d_{RH}, which limits the in-plane state area—the black region defined by the spatial dependence of magnetic anisotropy. Therefore, the $d_{RH}(y)$ boundary can be used for an estimation of the influence of the silver wedge thickness h on magnetic anisotropy. It has been found that the best fit of the bright region right side boundary $d_{RH}(y)$ shape (see Fig. 3) has the exponential $\exp(-h/h^*)$ dependence of magnetic anisotropy parameters, where h^* is a characteristic silver layer thickness. The boundaries of the reorientation region, determined by the relation $K_{1\text{eff}}(x, y, h^*) = 0$, are plotted in Fig. 3 as dashed lines for $h^* = 0.5$, 1, and 1.5 nm, taking the magnetic anisotropy constants for the silver and gold regions. The curve calculated for $h^* = 1$ nm describes the d_{RH} boundary in the best way.

One can determine the spatial distribution of the local coercivity field by analyzing domain wall positions during the magnetization reversal process. Let us consider the process induced by $H_\perp > 0$ for a fully saturated sample by $H_\perp < 0$. Domains with magnetization $M > 0$ nucleate, then their volumes increase at low coercivity regions—near $d_{RL}(y)$ and $d_{RH}(y)$. These domain walls, which can be named as "coercivity walls," move into regions of higher coercivity, mainly from a high d region, as shown in Fig. 3. This magnetization reversal process is characterized by a magnetic after-effect similar to the one reported in [16,17]. Three contributions determining the shape of the "coercivity wall" are present: (i) coercivity distribution forced by the overlayer designed geometry, (ii) coercivity distortion due to existing growth imperfections (e.g., visible at the silver region for the wall obtained at 115 Oe and in the vicinity of the sample edge in the gold region), and (iii) temporal randomness of domain wall motion during the magnetization reversal process [16] resulting in roughness of the wall. Therefore, averaging the randomness, investigation of the coercivity wall seems to be a very useful method for both a local coercivity study and localization of defects pinning the domain walls. Similar to the above spatial characterization of magnetic anisotropy constants, one can also describe the shape of the coercivity wall by the exponential dependence of local coercivity on h with about 1 nm characteristic thickness (see Fig. 3).

In the range of cobalt layer thickness between 1.3 nm (d_2 in the silver region) and 1.8 nm (d_1 in the gold region), RPT occurs while increasing h. The spatial variation of the magnetic anisotropy gives rise to perpendicular and in-plane domains, separated by a new type of overlayer-induced magnetic 90° wall. To our knowledge, a domain wall of this kind has not been studied before. Figure 4 illustrates the simulated spatial behavior of this wall for cobalt and silver wedges sloped along the x and y directions, respectively. Two edges of the wall are shown as a thin line $y_1[d(x)]$ [calculated as $K_{1\text{eff}}(x, y_1) = 0$], and a thick one $y_2[d(x)]$ [$K_{1\text{eff}}(x, y_2) = -2K_2(y_2)$]. Wall width $\Delta_W = y_2 - y_1$ strongly depends on d; it diverges to infinity approaching d_2^{Ag} thickness and achieves minimal value at d_1^{Au}. The domain wall width thus can be tuned by a gradient of the silver wedge—the higher the gradient, the narrower the wall—even down to nanometer size. The possibility of overlayer tuning of the anisotropy-constrained magnetic domain wall seems to be greater than the very recently reported [13] wall confinement given by a laterally modulated substrate. The wall is analyzed using a simple model of homogenous magnetization rotation. A more complicated spatial magnetization distribution study should be

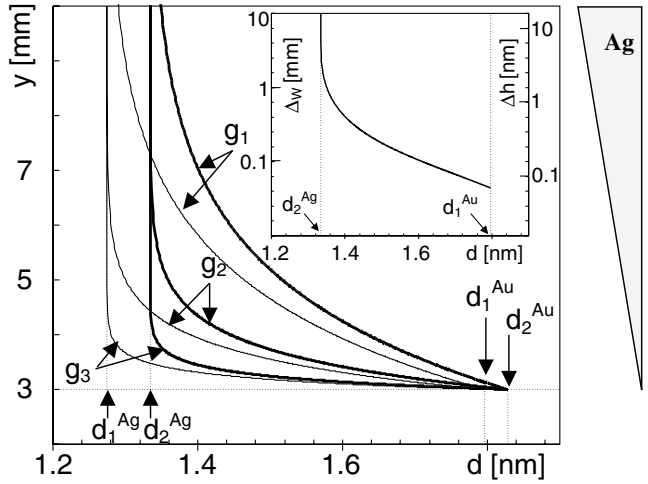

FIG. 4. The silver overlayer-constrained domain wall. The edge of the wall: y_1 (thin line) and y_2 (thick line) are drawn as a function of d. Double wedge geometry similar to that in the experiment was assumed: (i) the silver wedge starts at $y = 3$ mm (with three gradients $g_1 = 0.5 \times 10^{-6}$, $g_2 = 1.5 \times 10^{-6}$, $g_3 = 4.5 \times 10^{-6}$); (ii) the cobalt wedge is along x. Parameters describing the magnetic anisotropy were taken from Fig. 2. The inset shows the 90° wall width Δ_W ($= y_2 - y_1$) as a function of the x position, calculated for silver gradient $g_2 = 1.5 \times 10^{-6}$ (the right y axis shows the Δh difference of the silver thickness at the beginning and the end positions of the wall).

developed taking into consideration the wall size and local changes of anisotropy and coercivity fields.

In order to explain the observed influence of the silver cover layer on magnetic and magneto-optical properites of ultrathin Co film, one should consider modification of the electronic Co band structure due to the interfacial zone, where electronic structure is affected by hybridization of electronic wave function at the interface and/or confinement of the electronic states within the potential barriers at the interface. An extension of spin density calculations [18] performed for a Au covered Co monolayer on Au(111) seems to be promising for this purpose. An alloying mechanism also should be considered because due to silver and gold mutual solubility [19], the Ag-Au ''surface alloy'' is formed at the interface. For increasing h, the contribution of Ag atoms becomes more important. Complementary studies, both *in situ* (especially analysis of the initial stage of interface formation) and *ex situ*, supported by theoretical considerations are necessary for explanation of these phenomena.

In conclusion, a tunable magnetic structure was created based on chemically homogeneous ultrathin cobalt film by inducing—through a nonmagnetic overlayer—spatial modification of (i) the coercivity field, (ii) magnetic anisotropy, and (iii) magneto-optical parameters. A new type of overlayer-constrained magnetic domain wall, with easy tunable width, has been identified. The wall is different than classical walls and could rather be compared with a substrate constrained one [13]. Combined magneto-optical millimagnetometric and remnant state micromagnetometric studies (with millimeter and micrometer probing size, respectively) have been efficiently performed. New, high quality technologies of light detectors combined with image processing make the prospect of further development of magneto-optical micromagnetometric techniques very promising. Similar overlayer constraint of magnetic and magneto-optical properties could be extended to other than Co thin film systems. This magnetic properties tuning technique seems to be important from both the general physics and application points of view, especially because of the new possibilities for magnetic film patterning.

The authors thank Professor H. Szymczak for the work stimulation and discussions. This work was supported by the Polish State Committee for Scientific Research (Grant No. 2P03B 065 15) and ESF NANOMAG project.

*To whom correspondence should be addressed.
Email address: magnet@uwb.edu.pl

[1] *Ultrathin Magnetic Structures*, edited by B. Heinrich and J. A. C. Bland (Springer, Berlin, 1994), and references therein.
[2] R. Allenspach and A. Bischof, Phys. Rev. Lett. **69**, 3385 (1992).
[3] M. Speckmann, H. P. Oepen, and H. Ibach, Phys. Rev. Lett. **75**, 2035 (1995); H. Oepen *et al.*, Phys. Rev. B **55**, 2752 (1997).
[4] W. Weber *et al.*, Nature (London) **374**, 788 (1995); W. Weber *et al.*, Phys. Rev. Lett. **76**, 3424 (1996).
[5] S. Hope *et al.*, Phys. Rev. Lett. **80**, 1750 (1998).
[6] P. Beauvillain *et al.*, J. Appl. Phys. **76**, 6078 (1994).
[7] B. N. Engel *et al.*, J. Appl. Phys. **75**, 6401 (1994).
[8] T. Duden and E. Bauer, Phys. Rev. B **59**, 468 (1999).
[9] K. Hyomi *et al.*, Appl. Phys. Lett. **80**, 282 (2002).
[10] M. Dreyer *et al.*, Phys. Rev. B **59**, 4273 (1999).
[11] J. Kim *et al.*, Appl. Phys. Lett. **79**, 93 (2001).
[12] C. Chappert *et al.*, Science **280**, 1919 (1998).
[13] S. P. Li *et al.*, Phys. Rev. Lett. **88**, 087202 (2002).
[14] T. Shibauchi *et al.*, Phys. Rev. Lett. **87**, 267201 (2001); L. Krusin-Elbaum *et al.*, Nature (London) **410**, 444 (2001).
[15] Š. Višňovsky *et al.*, J. Magn. Magn. Mater. **128**, 179 (1993).
[16] J. Ferré *et al.*, Phys. Rev. B **55**, 15 092 (1997).
[17] *Spin Dynamics in Confined Magnetic Structures I*, edited by B. Hillebrands and K. Ounadjela, Topics in Applied Physics Vol. 83 (Springer-Verlag, Berlin, 2002), and references therein.
[18] B. Ujfalussy, L. Szunyogh, P. Bruno, and P. Weinberger, Phys. Rev. Lett. **77**, 1805 (1996).
[19] T. B. Massalski, Binary Alloy Diagrams, Ohio, 1986.